arXiv:hep-ph/0010334v1 30 Oct 2000

Charm quark mass from QCD sum rules for the charmonium system

M. Eidemüller and M. Jamin

Institut für Theoretische Physik, Universität Heidelberg,

Philosophenweg 16, 69120 Heidelberg, Germany

Abstract

In this work, the charm quark mass is obtained from a QCD sum rule analysis of the charmonium system. In our investigation we include results from nonrelativistic QCD at next-to-next-to-leading order. Using the pole mass scheme, we obtain a value of $M_c = 1.70 \pm 0.13$ GeV for the charm pole mass. The introduction of a potential-subtracted mass leads to an improved scale dependence. The running $\overline{\mathrm{MS}}$-mass is then determined to be $m_c(m_c) = 1.23 \pm 0.09$ GeV.

1   Introduction

Quantum Chromo Dynamics (QCD), describing the strong interactions, is one of the key components of the Standard Model. The determination of its parameters remains an essential task within modern particle physics. Much effort has therefore been put into the study of quark masses. However, in most cases where the system is sensitive to mass effects, also confinement plays an important role. Apart from the top mass, the quark masses can thus only be calculated by nonperturbative methods like QCD sum rules [1–3], lattice QCD [4, 5] or chiral perturbation theory [6, 7].

In the past, QCD moment sum rule analyses have been successfully applied for extracting the charm and bottom quark masses from experimental data on the charmonium and bottonium systems respectively. The fundamental quantity in these investigations is the vacuum polarisation function $\Pi(q^2)$:

$$\Pi_{\mu\nu}(q^2) = i \int d^4x \; e^{iqx} \, \langle T\{j_\mu(x)j_\nu(0)\}\rangle = (q_\mu q_\nu - g_{\mu\nu}q^2)\,\Pi(q^2)\,, \qquad (1)$$

where in the charm case the vector current is represented by $j_\mu(x) = (\bar{c}\gamma_\mu c)(x)$. Via the optical theorem, the experimental cross section $\sigma(e^+e^- \to c\bar{c})$ is related to the imaginary part of $\Pi(s)$:

$$R(s) = \frac{1}{Q_c^2} \frac{\sigma(e^+e^- \to c\bar{c})}{\sigma(e^+e^- \to \mu^+\mu^-)} = 12\pi \operatorname{Im}\Pi(s + i\epsilon)\,. \qquad (2)$$

Using a dispersion relation, we can express the moments $\mathcal{M}_n$ of $\Pi(s)$ by integrals over the spectral density $R(s)$:

$$\mathcal{M}_n = \frac{12\pi^2}{n!}\left(4m^2\frac{d}{ds}\right)^n \Pi(s)\Big|_{s=0} = \left(4m^2\right)^n \int_{s_{min}}^{\infty} ds\, \frac{R(s)}{s^{n+1}}\,. \qquad (3)$$

For convenience, we have defined the moments as dimensionless quantities. In addition, it will prove useful to express the moments by integrals over the velocity $v = \sqrt{1 - 4m^2/s}$:

$$\mathcal{M}_n = 2 \int_0^1 dv\, v(1 - v^2)^{n-1} R(v)\,. \qquad (4)$$

The moments can either be calculated theoretically, including perturbation theory, Coulomb resummation and nonperturbative contributions, or can be obtained from experiment. In this way, we can relate the charm quark mass to the hadronic properties of the charmonium system.

During the last years, several analyses for the bottonium system have been performed [8–15]. In these investigations, it turned out that the largest theoretical contributions arise from the threshold expansion in the framework of nonrelativistic QCD (NRQCD) which is known up to next-to-next-to-leading order (NNLO) [12, 14, 16]. The correlator can be expressed in terms of a Greens function, which shows a continuous spectrum above threshold, but also contains poles below threshold.

Yet these new theoretical developments have not been applied to the charmonium system. Due to the low scales involved, the analysis becomes more delicate here. We have therefore introduced a new method of analysis which allows for investigation of the influence of the individual contributions on the error. In particular, we have taken special care in obtaining the pole contributions and the reconstruction of the spectral density above threshold.

So far, we have not specified the mass definition to be used in eq. (3). A natural choice for this mass is the pole mass M. In the first part of our numerical analysis, we will use the pole mass scheme to extract the charm pole mass. However, as the pole mass suffers from renormalon ambiguities [17], it can only be determined up to corrections of order Λ_{QCD}. In the second part of our analysis we shall therefore use the recently introduced potential-subtracted mass m_{PS} [18]. From this mass definition we can obtain the $\overline{\text{MS}}$-mass more accurately than from the pole mass scheme.

In the next section, we shall present the contributions from the threshold expansion in the framework of NRQCD. The perturbative expansion which is needed for the reconstruction of the spectral density will be discussed in section 3. Afterwards, we will shortly describe the nonperturbative contributions and the phenomenological spectral function. In the numerical analysis, we shall first explain the method of analysis. We will then obtain the pole mass and the $\overline{\text{MS}}$-mass from an analysis of the pole mass and the PS-mass scheme respectively. The origin of different contributions to the error will be carefully investigated. We shall conclude with a summary and an outlook.

2 Coulomb resummation

Close to threshold, it turns out that the relevant expansion parameter is α_s/v rather than α_s since the velocity becomes of order α_s. These terms can be resummed in the framework of NRQCD and give the largest contributions to the theoretical moments.

The correlator is then expressed in terms of a Greens function [12, 19]:

$$\Pi(s) = \frac{N_c}{2M^2} \left(C_h(\alpha_s) G(k) + \frac{4k^2}{3M^2} G_C(k) \right) , \tag{5}$$

where $k = \sqrt{M^2 - s/4}$ and M represents the pole mass. The constant $C_h(\alpha_s)$ is a perturbative coefficient which is needed for the matching between the full and the nonrelativistic theory. It naturally depends on the hard scale. The Greens function is analytically known up to NNLO [12] and sums up terms of order α_s^n/v^{n-k} for $n \geq 0$ and $k = 1, 2, 3$. It is crucial for the analysis that the result depends on three scales. While the hard scale μ_{hard} is responsible for the hard perturbative processes, the soft scale μ_{soft} governs the expansion of the Greens function. Furthermore, the factorisation scale μ_{fac} separates the contributions of large and small momenta and plays the role of an infrared cutoff.

The Greens function contains two parts: the continuum above and the poles below threshold respectively. We are interested in both contributions separately: first, the individual corrections can be analysed and their error estimated. Second, in our numerical analysis we will reconstruct the spectral density above threshold and we thus need the corresponding spectral density at low velocities. In principle, the expressions for the energies and decay widths of the poles have been calculated. However, in the actual case of the charm quark the expansion does not converge well. We will therefore choose a different method of evaluation [20, 21]. Since the expansion for the Greens function at NNLO is known analytically [12], we can evaluate their contribution to the moments numerically by performing the derivatives. On the other hand, by using a dispersion relation, we can derive the continuum from the imaginary part of the correlator. From the difference we can then obtain the pole contributions:

$$\mathcal{M}_n^{Poles} = \frac{12\pi^2}{n!} \left(4M^2 \frac{d}{ds}\right)^n \Pi(s)\Big|_{s=0} - 12\pi \left(4M^2\right)^n \int_{4M^2}^{\infty} ds \, \frac{\text{Im}\,\Pi(s)}{s^{n+1}}. \quad (6)$$

Since we will not evaluate the poles near threshold, but rather calculate their contributions to the moments in a region where perturbation theory is expected to be valid, the convergence of the pole contributions is improved. Nevertheless, the poles will give the largest contribution to the theoretical moments and thus the dependence on the scales will remain relatively strong. In the numerical analysis we will give a detailed account on the size and behaviour of these contributions.

The large corrections are partly due to the definition of the pole mass. These contributions can be reduced by using an intermediate mass definition. In this analysis we will use the so-called potential-subtracted (PS) mass [18] where the potential below a separation scale μ_{sep} is subtracted:

$$m_{PS}(\mu_{sep}) = M - \delta m(\mu_{sep}), \quad \delta m(\mu_{sep}) = -\frac{1}{2} \int_{|\mathbf{q}| < \mu_{sep}} \frac{d^3 q}{(2\pi)^3} \, V(q). \quad (7)$$

3

Since the QCD potential contains the same renormalon ambiguities as the pole mass, in the difference they are cancelled. This mass definition thus leads to an improved scale dependence and a more precise determination of the $\overline{\text{MS}}$-mass.

3 Perturbative expansion

The perturbative spectral function $R(s)$ can be expanded in powers of the strong coupling constant α_s,

$$R^{Pt}(s) = R^{(0)}(s) + \frac{\alpha_s}{\pi} R^{(1)}(s) + \frac{\alpha_s^2}{\pi^2} R^{(2)}(s) + \dots . \tag{8}$$

From this expression the corresponding moments $\mathcal{M}_n^{Pt}$ can be calculated via the integral of eq. (4). The first two terms are known analytically and can for example be found in ref. [8]. $\Pi^{(2)}(s)$ is still not fully known analytically. However, the method of Padé-approximants has been exploited to calculate $\Pi^{(2)}$ numerically, using available results at high energies, analytical results for the first eight moments and the known threshold behaviour [22, 23]. This information is sufficient to obtain a numerical approximation of $\Pi^{(2)}(s)$ in the full energy range.

The numerical stability of the results can be checked in different ways. By choosing different Padé-approximants or by selecting a smaller set of input data the results for the moments remain almost unchanged. Furthermore, some contributions to the spectral density like those from internal quark loops are known analytically and are in very good agreement with the numerical spectral density. This provides strong support that the numerically obtained spectral density gives a very good approximation to the exact spectral density.

4 Condensate contributions

The nonperturbative effects on the vacuum correlator are parametrised by the condensates. The leading correction is the gluon condensate contribution which is known up to next-to-leading order [24]. Furthermore, the dimension 6 and 8 contributions have been calculated and will be included in our analysis [25–27]. In the analysis below, we have employed a value of $\langle \alpha_s / \pi FF \rangle = 0.024 \pm 0.012 \text{ GeV}^4$ for the gluon condensate.

It will turn out that the condensate contributions are suppressed when compared to former charmonium sum rule analyses [28, 29] and only have

little influence on the mass. Besides an increase of the theoretical moments from the Coulomb contributions we will restrict the moments to $n \leq 7$ where the nonperturbative contributions are relatively small. Since we obtain a larger pole mass than the former analyses, the condensates, starting with a power of $1/M^4$, are suppressed further.

5 Phenomenological spectral function

Experimentally, the lowest lying six ψ-resonances have been observed. Since the widths of the poles are very small compared to the masses, the narrow-width approximation provides an excellent description of these states. To model the contributions of the hadronic continuum, we use the assumption of quark-hadron-duality and integrate over the perturbative spectral density:

$$\frac{\mathcal{M}_n}{(4M^2)^n} = \frac{9\pi}{\alpha_{em}^2 Q_c^2} \sum_{k=1}^{6} \frac{\Gamma_k}{E_k^{2n+1}} + \int_{s_0}^{\infty} ds \frac{R^{Pt}(s)}{s^{n+1}} . \tag{9}$$

To estimate the continuum contribution we will use a threshold in the range of $3.6 \text{ GeV} \leq \sqrt{s_0} \leq 4.2 \text{ GeV}$ with a central value of $\sqrt{s_0} = 3.8 \text{ GeV}$. The lower value corresponds to using a perturbative continuum around the $\psi(2S)$ but nevertheless including the higher resonance contributions. This is certainly over-counting the continuum contribution. The higher value would assume no additional continuum contribution until the $\psi(5S)$ resonance. However, the most dominant phenomenological contributions come from the first two ψ-resonances resulting in a small influence of the continuum even for low values of n.

6 Numerical analysis

6.1 Method of analysis

Besides the contributions from the poles of the Greens function and the condensates, the theoretical part of the correlator contains the spectral density above threshold. Now we will discuss the different parts of the spectral density. A more detailed description of our procedure will be presented in a forthcoming publication [30].

For high velocities the spectral density is well described by the perturbative expansion where we have fixed the hard scale to the pole mass. However, as one approaches smaller values of v, the perturbative expansion breaks down. The resummed spectral density, on the other hand, gives a good description for low values of v, but becomes unreliable for high velocities. For
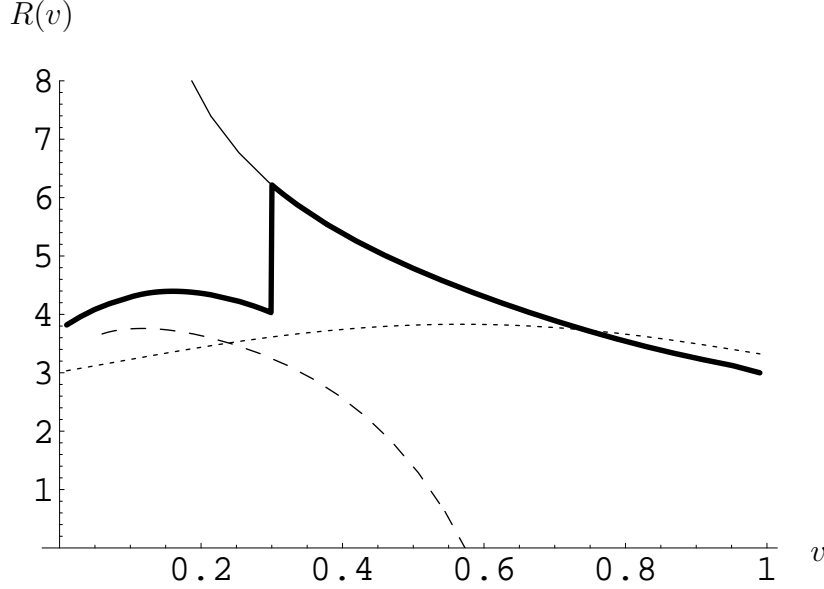
Figure 1: Thick solid line: reconstructed spectral density; Thin solid line: perturbative spectral density; dotted line: perturbation theory at NLO; dashed line: resummed spectral density.

these reasons, we will introduce a separation velocity $v_{sep} \approx 0.3$. Above v_{sep} we will use the perturbative spectral density. Below v_{sep}, we take the resummed spectral density adding the terms which are included in perturbation theory but not in resummation.

In fig. 1 we have displayed the different contributions. The dotted line represents the perturbative expansion at NLO. The thin solid line also includes the NNLO. Whereas for high velocities the perturbative expansion is well convergent, the importance of the higher corrections increases for smaller v. The dashed line is the resummed spectral density and the thick solid line the reconstructed spectral density. For the charmonium system, there exists a range of intermediate values of v where neither the perturbative expansion nor the resummation can be trusted. Indeed, it can be clearly seen that the reconstructed spectral density shows a gap at the separation velocity. To estimate the error we have varied v_{sep} between 0.2 and 0.4. The analysis shows that though the introduction of the separation velocity stabilises the sum rules, the variation only has a minor influence on the mass.
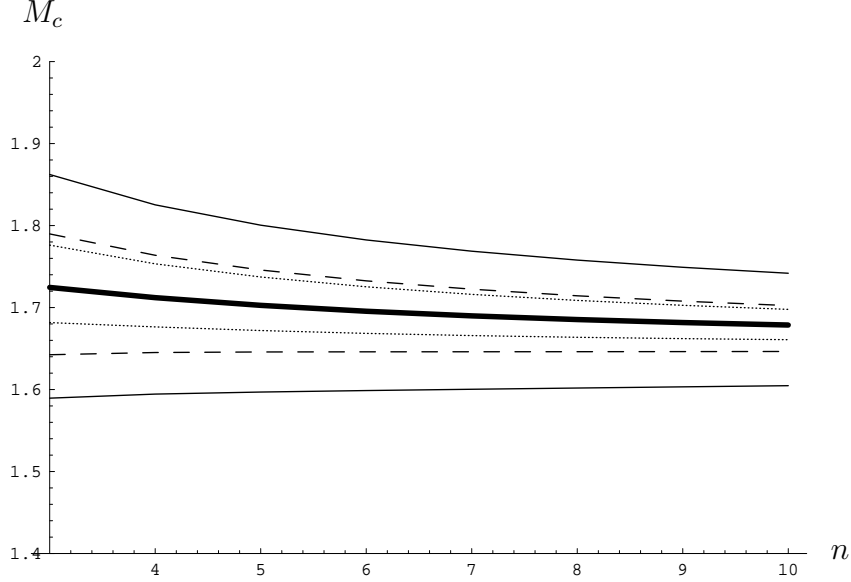
M_c

Figure 2: Thick solid line: central pole mass; thin solid lines: M_c for $\mu_{soft} = 1.05$ and 1.5 GeV; dashed lines: M_c for $\mu_{fac} = 1.2$ and 1.7 GeV; dotted lines: M_c for $\mu_{hard} = 1.4$ and 2.5 GeV.

6.2   Pole mass scheme

Since the threshold region becomes more important for larger values of n, as can already be seen from the factor $(1 - v^2)^{n-1}$ of eq. (4), also the NLO and NNLO corrections grow for larger n. We will therefore restrict our analysis to moments with $n \leq 7$. As our method of analysis needs moments of $n \geq 3$ to reconstruct the spectral density, we will use $3 \leq n \leq 7$. Since the continuum part of the phenomenological spectral density is relatively small even for low values of n, it does not set a lower bound on n. As central values for our scales we have selected:

$$\mu_{soft} = 1.2 \text{ GeV}, \quad \mu_{fac} = 1.45 \text{ GeV}, \quad \mu_{hard} = 1.7 \text{ GeV}. \tag{10}$$

We have set the hard scale equal to the central value for the pole mass. For the soft scale, we would have liked to choose a value around $\mu_{soft} \sim 0.8 - 0.9$ GeV, but the NNLO corrections get out of control for these scales. Thus, we take a central value of $\mu_{soft} = 1.2$ GeV and vary it in an interval of $1.05 \text{ GeV} \leq \mu_{soft} \leq 1.5 \text{ GeV}$. The factorisation scale separates the different regions and should lie between the two other scales.

In table 1 we have collected the individual moments for different values of n. $\mathcal{M}_n^{Poles}$ are the theoretical poles of the Greens function, $\mathcal{M}_n^{NRResum}$ the

7

n	3	4	5	6	7
$\mathcal{M}_n^{Poles}$	3.84	4.44	5.11	5.87	6.73
$\mathcal{M}_n^{Pt}$	1.92	1.55	1.32	1.15	1.03
$\mathcal{M}_n^{NRResum}$	0.28	0.27	0.26	0.24	0.23
$\mathcal{M}_n^{Counter}$	0.69	0.66	0.64	0.62	0.60
$\mathcal{M}_n^{Continuum}$	0.75	0.47	0.31	0.21	0.15
$\mathcal{M}_n^{Condensates}$	-0.03	-0.05	-0.06	-0.08	-0.09

Table 1: Moments for different n with the parameters $\mu_{soft} = 1.2$ GeV, $\mu_{fac} = 1.45$ GeV, $\mu_{hard} = 1.7$ GeV, $\sqrt{s_0} = 3.8$ GeV and $v_{sep} = 0.3$.

μ_{soft}	1.05	1.1	1.2	1.3	1.4	1.5
$\mathcal{M}_5^{Poles}$	9.50	7.52	5.14	3.80	2.97	2.41
μ_{fac}	1.2	1.3	1.4	1.5	1.6	1.7
$\mathcal{M}_5^{Poles}$	6.79	6.12	5.46	4.82	4.18	3.55
μ_{hard}	1.4	1.5	1.6	1.8	2.0	2.5
$\mathcal{M}_5^{Poles}$	4.24	4.62	4.93	5.45	5.85	6.56

Table 2: Pole moments with $n = 5$ for different μ_{soft} with $\mu_{fac} = 1.45$ GeV and $\mu_{hard} = 1.7$ GeV, for different μ_{fac} with $\mu_{soft} = 1.2$ GeV and $\mu_{hard} = 1.7$ GeV and for different μ_{hard} with $\mu_{soft} = 1.2$ GeV and $\mu_{fac} = 1.45$ GeV.

moments from the nonrelativistic spectral density and $\mathcal{M}_n^{Counter}$ contains the double counted terms from the perturbative expansion below v_{sep}. In this scheme the theoretical moments are dominated by the pole contributions. Though the size of these terms grow with larger n, the mass remains relatively stable since the contributions of the moments to the mass is suppressed by a power of $1/2n$.

The thick solid line in fig. 2 shows the central value for the pole mass $M_c = 1.70$ GeV with the parameters from eq. (10). The error is dominated by the variation of the scales. We obtain:

$$1.05 \text{ GeV} \leq \mu_{soft} \leq 1.5 \text{ GeV} : \qquad \Delta M_c = 100 \text{ MeV} ,$$
$$1.2 \text{ GeV} \leq \mu_{fac} \leq 1.7 \text{ GeV} : \qquad \Delta M_c = 50 \text{ MeV} ,$$
$$1.4 \text{ GeV} \leq \mu_{hard} \leq 2.5 \text{ GeV} : \qquad \Delta M_c = 40 \text{ MeV} . \qquad (11)$$

In particular, in table 2 we have listed the influence of the scales on the pole contributions. We have varied the scales within physically reasonable ranges. Since the convergence of the nonrelativistic expansion is not very good for the charmonium system, the scales cannot be chosen arbitrarily

μ_{soft}		1.05	1.1	1.2	1.3	1.4	1.5
	LO	3.03	2.57	1.95	1.56	1.29	1.10
$\mathcal{M}_5^{Poles}$	NLO	5.60	4.75	3.61	2.89	2.40	2.04
	NNLO	9.50	7.52	5.14	3.80	2.97	2.41
	LO	0.64	0.61	0.57	0.54	0.51	0.49
$\mathcal{M}_5^{NRResum}$	NLO	0.24	0.27	0.29	0.30	0.31	0.31
	NNLO	0.31	0.28	0.23	0.20	0.18	0.17

Table 3: Size of the moments from the poles and the resummed spectral density at LO, NLO and NNLO for different values of μ_{soft}.

Source	ΔM_c
Variation of μ_{soft}	100 MeV
Variation of μ_{fac}	50 MeV
Variation of μ_{hard}	40 MeV
Threshold s_0	10 MeV
Experimental error	15 MeV
Variation of v_{sep}	10 MeV
Variation of Λ_{QCD}	50 MeV
Total error	130 MeV

Table 4: Single contributions to the error of M_c.

far away from their central values. Though the analysis is stable inside the given intervals, the expressions tend to become unstable for scales outside of the chosen ranges. In table 3 we have confronted the NLO and NNLO corrections to the LO. The NNLO corrections turn out not to be so large for values of $\mu_{soft} \geq 1.2$ GeV. But this may happen accidentally since there are cancellations for the combination of scales used in this analysis. Therefore this should not be taken as an indication for small higher order corrections. In order to obtain a more conservative estimate, thus we have used the variation of the scales in our error analysis.

A significant uncertainty also comes from Λ_{QCD}. By choosing $\Lambda_{QCD} = 330 \pm 30$ MeV we get an error of $\Delta M_c = 50$ MeV. The variation of the continuum threshold s_0 and the error from the experimentally measured decay widths only have a small influence on the mass. We have summarised the results in table 4. Adding the errors in quadrature we obtain the charm pole mass:
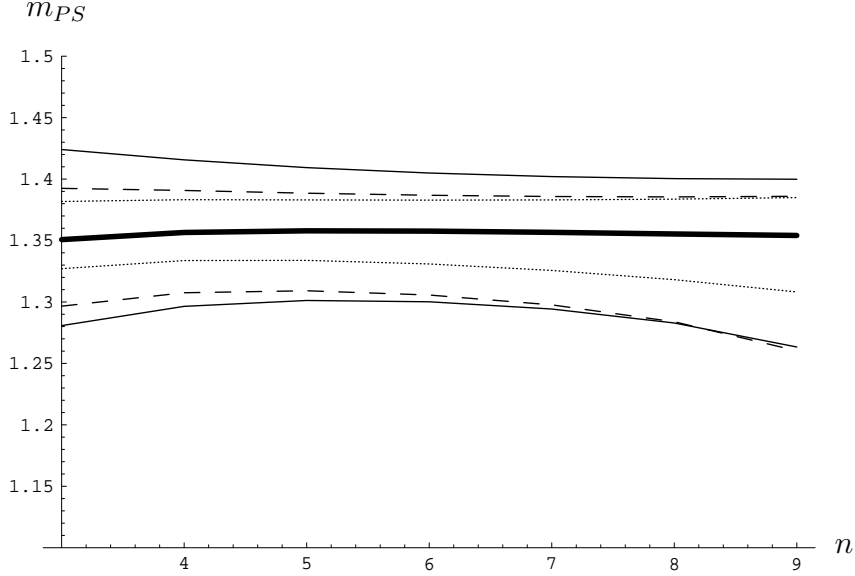
$$M_c = 1.70 \pm 0.13 \text{ GeV} . \tag{12}$$

Figure 3: Thick solid line: central PS-mass; thin solid lines: m_{PS} for $\mu_{soft} = 1.05$ and 1.5 GeV; dashed lines: m_{PS} for $\mu_{fac} = 1.2$ and 1.7 GeV; dotted lines: m_{PS} for $\mu_{hard} = 1.4$ and 2.5 GeV.

Using the three-loop relation between the pole and the $\overline{\text{MS}}$-mass which has been calculated recently [31, 32], we obtain $m_c(m_c) = 1.20 \pm 0.13$ GeV for the $\overline{\text{MS}}$-mass. In addition, we get an error from the perturbative relation between the two masses which does not converge for the charm case and can be of order Λ_{QCD}. By using the PS-mass, in the next section we will derive a more precise value for the $\overline{\text{MS}}$-mass.

6.3 Potential-subtracted mass scheme

First, we have to choose a value for the separation scale μ_{sep}. This scale should be taken large enough in order to guarantee a perturbative relation to the $\overline{\text{MS}}$-mass. On the other hand, it should be smaller than Mv. Both conditions cannot be well fulfilled at the same time. As a compromise value we will choose $\mu_{sep} = 1.0 \pm 0.2$ GeV. In this scheme, the pole contributions from the Greens function turn out to be smaller than in the pole mass scheme. The contributions from the condensates get more important here and we shall restrict our analysis to $n \leq 6$ to where these corrections are under good control.

Using the same central values for the scales (10) we obtain $m_{PS}(\mu_{sep} = 1.0) = 1.35$ GeV and from this value a $\overline{\text{MS}}$-mass of $m_c(m_c) = 1.23$ GeV.

n	3	4	5	6
$\mathcal{M}_n^{Poles}$	0.59	0.40	0.27	0.19
$\mathcal{M}_n^{Pt}$	1.16	0.83	0.63	0.49
$\mathcal{M}_n^{NRResum}$	0.33	0.32	0.30	0.29
$\mathcal{M}_n^{Counter}$	0.53	0.47	0.42	0.37
$\mathcal{M}_n^{Continuum}$	0.42	0.20	0.09	0.03
$\mathcal{M}_n^{Condensates}$	-0.07	-0.09	-0.12	-0.14

Table 5: Moments for different n with the parameters $\mu_{soft} = 1.2$ GeV, $\mu_{fac} = 1.45$ GeV, $\mu_{hard} = 1.7$ GeV, $\sqrt{s_0} = 3.8$ GeV and $v_{sep} = 0.3$.

μ_{sep}	0.8	0.9	1.0	1.1	1.2
m_{PS}	1.38	1.36	1.35	1.34	1.33
$m_c(m_c)$	1.20	1.22	1.23	1.24	1.26

Table 6: Change of the masses for different values of μ_{sep}.

The introduction of the intermediate mass definition leads to a reduced scale dependence:

$$
\begin{aligned}
1.05 \text{ GeV} \le \mu_{soft} \le 1.5 \text{ GeV} : & \qquad \Delta m_{PS} = 60 \text{ MeV} , \\
1.2 \text{ GeV} \le \mu_{fac} \le 1.7 \text{ GeV} : & \qquad \Delta m_{PS} = 40 \text{ MeV} , \\
1.4 \text{ GeV} \le \mu_{hard} \le 2.5 \text{ GeV} : & \qquad \Delta m_{PS} = 30 \text{ MeV} . \qquad (13)
\end{aligned}
$$

In table 5 we again have collected the moments for different values of n. The influence of the pole contributions is clearly reduced and becomes even smaller for higher values of n. Since we have chosen the separation scale relatively large in comparison to Mv, the PS-mass lies a good deal lower than the pole mass and we are further away from the threshold region. The convergence of the perturbative expansion is improved in this scheme as well. In table 6 we have varied the separation scale μ_{sep} between $0.8 \text{ GeV} \le \mu_{sep} \le 1.2$ GeV. The error on the $\overline{\text{MS}}$-mass is about 30 MeV. The change of the two masses is not directly correlated since the variation of μ_{sep} also changes the relation between the masses. When compared to the pole mass scheme, the uncertainty from α_s is reduced and the influence of the condensates becomes more important here.

In table 7 we have listed the individual contributions to the error of m_{PS} and m_c. Finally, we obtain the masses:

$$
\begin{aligned}
m_{PS}(\mu_{sep} = 1.0) &= 1.35 \pm 0.09 \text{ GeV} , \\
m_c(m_c) &= 1.23 \pm 0.09 \text{ GeV} . \qquad (14)
\end{aligned}
$$

11

Source	Δm_{PS}	Δm_c
Variation of μ_{soft}	60 MeV	50 MeV
Variation of μ_{fac}	40 MeV	40 MeV
Variation of μ_{hard}	30 MeV	30 MeV
Variation of μ_{sep}	30 MeV	30 MeV
Threshold s_0	30 MeV	30 MeV
Experimental error	10 MeV	10 MeV
Condensates	20 MeV	20 MeV
Variation of v_{sep}	10 MeV	10 MeV
Variation of Λ_{QCD}	10 MeV	20 MeV
Total error	90 MeV	90 MeV

Table 7: Single contributions to the error of m_{PS} and m_c.

When we compare this value of the $\overline{\text{MS}}$-mass to the one from the last section, $m_c(m_c) = 1.20$ GeV, we see that the central value remains almost unchanged. This is not self-evident, as the dominating pole contributions are reduced in the PS-scheme and the relative influence of the individual contributions is shifted.

7   Conclusions

To summarise, our values obtained for the charm quark pole- and $\overline{\text{MS}}$-mass are as follows:

$$
\begin{aligned}
M_c &= 1.70 \pm 0.13 \text{ GeV}, \\
m_c(m_c) &= 1.23 \pm 0.09 \text{ GeV}.
\end{aligned}
\tag{15}
$$

The obtained value for the pole mass lies somewhat higher than in previous sum rule analyses [28, 29]. In [28] the authors used perturbation theory to NLO resulting in a value of $M_c = 1.46 \pm 0.07$ GeV. In the second investigation [29, 33] the analysis has been performed in the $\overline{\text{MS}}$-scheme with perturbation theory to NLO. Using the NLO relation to the pole mass the author obtains $m_c(m_c) = 1.26 \pm 0.05$ GeV and $M_c = 1.42 \pm 0.03$ GeV. The author has also performed an analysis using resummation in LO with a value of $M_c = 1.45 \pm 0.07$ GeV.

In our analysis the increased value of the pole mass is essentially due to large Coulomb contributions which have not been included in former analyses. As a consequence, the error becomes larger as well. In a recent analysis, the pole mass has been estimated from the charmonium ground state at

NNLO [16]. Here the authors obtained a pole mass of $M_c = 1.88^{+0.22}_{-0.13}$ GeV. This value resulted from large corrections of the Coulomb potential to the ground state.

During the last years, several lattice analyses obtained the following values for the $\overline{\text{MS}}$-mass:

$$
\begin{aligned}
m_c(m_c) &= 1.59 \pm 0.28 \text{ GeV} & [34] \,, \\
m_c(m_c) &= 1.33 \pm 0.08 \text{ GeV} & [35] \,, \\
m_c(m_c) &= 1.73 \pm 0.26 \text{ GeV} & [36] \,, \\
m_c(m_c) &= 1.22 \pm 0.05 \text{ GeV} & [37, 38] \,.
\end{aligned}
\tag{16}
$$

Whereas the results from $[35, 37, 38]$ are in good agreement with this analysis, the investigations from [34] and [36] obtain higher masses. For the time-being, the results are not conclusive and future lattice calculations for the charm mass might be of interest. Since other methods reveal significant uncertainties in the determination of the quark masses, QCD sum rules remain amongst the most precise tools to extract these fundamental quantities.

References

[1] M.A. Shifman, A.I. Vainshtein and V.I. Zakharov, *Nucl. Phys.* **B 147** (1979) 385, *Nucl. Phys.* **B 147** (1979) 448.

[2] L.J. Reinders, H. Rubinstein and S. Yazaki, *Phys. Rep.* **127** (1985) 1.

[3] S. Narison, *QCD Spectral Sum Rules, World Scientific* (1989).

[4] H.J. Rothe, *Lattice gauge theories, World Scientific* (1992).

[5] I. Montvay and G. Münster, *Quantum fields on a lattice, Cambridge University Press* (1994).

[6] J. Gasser and H. Leutwyler, *Nucl. Phys.* **B 250** (1985) 465.

[7] A. Pich, *Rept. Prog. Phys.* **58** (1995) 563.

[8] M. Jamin and A. Pich, *Nucl. Phys.* **B 507** (1997) 334.

[9] M.B. Voloshin, *Int. J. Mod. Phys.* **A 10** (1995) 2865.

[10] J.H. Kühn, A.A. Penin and A.A. Pivovarov, *Nucl. Phys.* **B 534** (1998) 356.

[11] K. Melnikov and A. Yelkhovsky, *Phys. Rev.* **D 59** (1999) 114009.

[12] A.A. Penin and A.A. Pivovarov, *Nucl. Phys.* **B 549** (1999) 217.

[13] M. Beneke and A. Signer, *Phys. Lett.* **B 471** (1999) 233.

[14] A.H. Hoang, *Phys. Rev.* **D 59** (1999) 014039.

[15] A.H. Hoang, *Phys. Rev.* **D 61** (2000) 034005.

[16] A. Pineda and F.J. Ynduráin, *Phys. Rev.* **D 58** (1998) 094022.

[17] M. Beneke, *Phys. Rep.* **317** (1999) 1.

[18] M. Beneke, *Phys. Lett.* **B 434** (1998) 115.

[19] M.J. Strassler and M.E. Peskin, *Phys. Rev.* **D 43** (1991) 1500.

[20] M. Eidemüller, *Dissertation, Heidelberg University* (2000).

[21] M. Eidemüller and M. Jamin, `hep-ph/0010133`.

[22] K.G. Chetyrkin, J.H. Kühn and M. Steinhauser, *Nucl. Phys.* **B 482** (1996) 213.

[23] K.G. Chetyrkin, J.H. Kühn and M. Steinhauser, *Nucl. Phys.* **B 505** (1997) 40.

[24] D.J. Broadhurst, P.A. Baikov, V.A. Ilyin, J. Fleischer, O.V. Tarasov and V.A. Smirnov, *Phys. Lett.* **B 329** (1994) 103.

[25] S.N. Nikolaev and A.V. Radyushkin, *Nucl. Phys.* **B 213** (1983) 285.

[26] S.N. Nikolaev and A.V. Radyushkin, *Phys. Lett.* **B 124** (1983) 243.

[27] D.J. Broadhurst and S.C. Generalis, *Phys. Lett.* **B 165** (1985) 175.

[28] C.A. Dominguez, G.R. Gluckman and N. Paver, *Phys. Lett.* **B 333** (1994) 184.

[29] S. Narison, *Phys. Lett.* **B 341** (1994) 73.

[30] M. Eidemüller and M. Jamin, *in preparation.*

[31] K. Melnikov and T. van Ritbergen, *Phys. Lett.* **B 482** (2000) 99.

[32] K.G. Chetyrkin and M. Steinhauser, *Nucl. Phys.* **B 573** (2000) 617.

[33] S. Narison, *Nucl. Phys.* **74** *(Proc. Suppl.)* (1999) 304.

[34] C.R. Allton, M. Ciuchini, M. Crisafulli, E. Franco, V. Lubicz and G. Martinelli, *Nucl. Phys.* **B 431** (1994) 667.

[35] A. Kronfeld, *Nucl. Phys.* **63** *(Proc. Suppl.)* (1998) 311.

[36] V. Giménez, L. Giusti, F. Rapuano and M. Talevi, *Nucl. Phys.* **B 540** (1999) 472.

[37] A. Bochkarev and P. de Forcrand, *Nucl. Phys.* **B 477** (1996) 489.

[38] A. Bochkarev and P. de Forcrand, *Nucl. Phys.* **53** *(Proc. Suppl.)* (1997) 305.